A Cyclonic Submesoscale Coherent Vortex in the Northeast Pacific*

Gregory C. Johnson

NOAA/Pacific Marine Environmental Laboratory, Seattle, Washington

Submitted 20 May 2008

as a Note to the *Journal of Physical Oceanography*

Corresponding author address: Dr. Gregory C. Johnson, NOAA/Pacific Marine Environmental Laboratory, 7600 Sand Point Way Bldg. 3, Seattle Washington 98115-6349.

E-mail : gregory.c.johnson@noaa.gov

*PMEL Contribution Number 3220

ABSTRACT

A cyclonic Submesoscale Coherent Vortex (SCV) sampled by a single temperature-salinity-pressure profile from an Argo float about 1200 km west of the southern end of Baja California is analyzed. A subsurface core of anomalously warm and salty water (about 0.35 saltier and 1.5°C warmer than nearby profiles from the same float) centered near potential density anomaly 26.5 kg m^{-3} is present within the SCV. The potential temperature-salinity anomaly decays vertically from this peak and is confined to about $26.2 < \sigma_\theta < 26.9$ kg m^{-3}, or 160 dbar in vertical extent. In addition to being warm and salty, the core of the feature is anomalously high in stratification, hence planetary potential vorticity (Π). This dynamical signature, which extends to at least 800 dbar, allows a geostrophic estimate of the cyclonic transport around the SCV of about 0.8×10^6 m^3 s^{-1}. Since it is uncertain if the profile of interest samples the core of the SCV, this transport estimate can be thought of as a lower bound. The transport estimate and the warm, salty character of the SCV are both consistent with an origin from the California Undercurrent (CU), a subsurface eastern boundary current that flows northward along the west coast of North America. However, the large values of Π within the SCV suggest that its formation process was not a conservative one, since the CU carries much lower Π waters northward from lower latitudes.

1. Introduction

Submesoscale Coherent Vortices (SCVs) are a distinct oceanic phenomenon. According to McWilliams (1985), SCVs can be characterized by a localized vertical structure usually with a subsurface vertical maximum in azimuthal velocity, a horizontal scale less than the first baroclinic radius of deformation, a primarily horizontal and circular flow field, and retention of core water properties for many rotation periods. SCVs can move long distances from their generation sites, so that their core properties can become anomalous relative to their surroundings. In addition, SCVs are usually anticyclonic, with a vertical stratification minimum at their core.

Here we present an analysis of Argo float Conductivity–Temperature-Depth (CTD) instrument data reported within an uncommon cyclonic SCV. This SCV has warm and salty potential temperature–salinity (θ–S) characteristics in its core suggesting an origin in the southern portions of the California Undercurrent (CU) and high planetary potential vorticity (Π) characteristics of unknown origin. While the sampling pattern of the Argo array, with its target of 3° lat. × 3° long. spacing between floats, and its nominal 10-day cycle between float profiles, is not designed to resolve eddies, some of the roughly 100,000 CTD profiles per year reported by the floats of the Argo array are located within eddies. The large number of high-quality CTD profiles available from Argo allows for an exploration of ocean eddies, albeit an under-resolved one in terms of the individual features.

The CU, the apparent source of the cyclonic SCV studied here, is an eastern boundary undercurrent that carries warm, salty, low Π, oxygen-poor, and nutrient-rich water of equatorial origin northward along the west coast of North America. The CU is a

fairly narrow feature, generally not extending beyond 100 km from the coast, with a high velocity core along the continental slope (Lynn and Simpson 1987). The CU has a subsurface core in velocity (as well as water property anomalies) near σ_θ = 26.5 kg m^{-3} and has been found along the west coast of America from at least Baja California to Vancouver Island (Lynn and Simpson 1987; Pierce et al. 2000). The CU has a pronounced seasonal cycle, being weakest in Boreal Spring with most extreme water properties slightly lagging the strongest velocity signature (Lynn and Simpson 1987). In addition, during El Niños, at any rate the very strong 1997–98 event, the equatorial characteristics of the CU appear intensified, and the CU strengthened (Durazo and Baumgartner 2002; Lynn and Bograd 2002; Collins et al. 2002).

An extensive set of velocity data collected during many short zonal ship transects across the shelf break of the west coast of North America from 33 – 51°N during July – August 1995, allows a core speed estimate of about 0.2 m s^{-1} for the CU, and a volume transport estimate of about 0.8×10^6 m^3 s^{-1} northward within a 125 – 325-m layer that spans some of the vertical extent of the CU (Pierce et al. 2000). A set of 19 bi-monthly sections taken between 1988 and 1991 off Point Sur, California allows a mean volume transport estimate of about 2.9×10^6 m^3 s^{-1} for the CU and an associated inshore surface-intensified countercurrent, which extend about 100 km from the shelf break in the mean (Collins et al. 2000). Analysis of the first 12 of these sections yields a mean volume transport estimate of 2.6×10^6 m^3 s^{-1} for the CU alone, with a springtime minimum during May sections (Castro et al. 2001).

The CU appears to shed anticyclonic subsurface eddies, perhaps through baroclinic instabilities (Simpson et al. 1984; Lynn and Simpson 1990). These eddies have been

observed in detailed surveys, and some of them have almost no surface velocity signature despite their robust subsurface expression and a size sometimes exceeding a baroclinic radius of deformation (Huyer et al. 1998). A subsurface anticyclonic eddy with water properties of the CU (a warm, salty, low-stratification core) has been observed as far south as northern Baja California (Jerónimo and Gómez-Valdés 2007). A strikingly anomalous subsurface lens of water with properties typical of the CU near Baja California (warm, salty, and oxygen-poor) has even been observed north of Hawaii (Lukas and Santiago-Mandujano 2001). Although that feature did not have a strong dynamic signature, a very slight reduction in stratification may have been present in its core.

Analysis of Lagrangian data from subsurface floats deployed near Monterey and San Francisco, California shows a strong CU signature of northward flow of 0.10 – 0.15 m s^{-1} within 100 km of the coast, with a predominance of anticyclonic submesoscale motions just offshore (Garfield et al. 1999). The floats caught in these anticyclonic features exhibit a slow (0.015 m s^{-1}) westward drift as they swirl around the SCVs with azimuthal velocities of about 0.10 – 0.15 m s^{-1}. Garfield et al. (1999) suggest that the apparently numerous SCVs shed from the CU may play a significant role in carrying subsurface warm, salty, oxygen-poor, nutrient-rich, low-stratification waters offshore.

However, cyclonic SCVs are apparently rare in the region, so one found in an Argo CTD profile is analyzed here. Following this introduction, the data used in the analysis are discussed along with gridding and mapping routines, as well as the method for estimation of a derived property (Section 2). Then results of the analysis are presented (Section 3). The paper ends with a discussion of the results (Section 4).

2. Data

Only Argo CTD profile data are used in this study. Data were downloaded from an Argo Global Data Assembly Center on 10 April 2008. When delayed-mode quality controlled data (adjusted values) are available, those are used. Otherwise, real-time quality controlled data (raw values) are used instead. Only data at pressures with pressure (P), temperature (T), and salinity (S) flagged as good (Argo quality flag 1) are retained in the analyses.

Some of the study involves analysis of data from individual floats including evaluating their potential temperature–salinity (θ–S) curves, contoured time-pressure sections of θ, S, and potential density anomaly (σ_θ), as well as geostrophic calculations. For these analyses, float T and S data from each profile are vertically interpolated to a regular 5-dbar pressure grid using a shape-preserving spline, assuming that the shallowest good values of T and S are representative of surface values. Derived quantities are estimated from the gridded values of T, S, and P. The Argo float most closely analyzed, that with WMO (World Metrological Organization) #4900452, reports samples at about 8-dbar intervals from about 5 to 160 dbar. Deeper than 160 dbar, the sampling intervals are about 0.05 of the sample pressures themselves for this float.

Additionally, properties on σ_θ surfaces (isopycnals) are analyzed here. For this analysis, any derived parameters desired are calculated from the float P, T, and S data. Then, the measured and derived parameters are linearly interpolated to desired isopycnals from each CTD profile used. The vertical distance over which interpolations are performed is retained for purposes of quality control.

For this study the derived parameter Π is estimated over a σ_θ layer bounded by 26.2 < σ_θ < 26.7 kg m^{-3} using

$$\Pi = \frac{f}{1000\ kg\ m^{-3} + \sigma_{\theta m}} \frac{\sigma_{\theta u} - \sigma_{\theta l}}{z_u - z_l}, \quad (1)$$

where *f* is the Coriolis parameter and *z* is the depth of a given σ_θ surface. The subscripts *u*, *l*, and *m* in (1) refer to the upper, lower, and mean values of the layer.

Properties on isopycnals or in isopycnal layers are mapped to a regular geographic grid using a lowess smoother with a 1000-km zonal and 500-km meridional scale. At each point on this grid, data within range of the smoother from that point are subject to the following screens: First, data interpolated over too large a pressure interval are discarded. The discard thresholds for interpolation intervals are values exceeding 22 dbar at the surface and 67 dbar at pressures of 300 dbar or greater. These thresholds range linearly from 22 to 67 dbar between the surface and 300 dbar. After that step, data that are more than the three times the distance of the interquartile range from either the first or third quartiles are discarded. The filter-weighted centers of the data, as well as the filter-weighted numbers of data, are also calculated for every grid point on each map. If the distance from the mapped grid point to the filter-weighted center of the data is either more than 1/3 of the range of the smoother, or if there are fewer than 150 filter-weighted observations, the map at the grid point in question is discarded because the data are either too distant or too few.

3. Results

We are responsible for delayed-mode scientific quality control of the data from

Argo floats deployed by NOAA's Pacific Marine Environmental Laboratory, including WMO #4900452. During this quality control process, an unusual feature was noticed in data from this float. Specifically, data from profile 67 of Argo float WMO #4900452 (observed on 10 December 2005 at 23.537°N and 121.619°W) show evidence for a cyclonic SCV. The θ–S curve from this profile contains a warm salty water-mass anomaly that is present neither in previous nor subsequent profiles (Figure 1). The θ–S anomaly is largest near σ_θ = 26.5 kg m^{-3}, approaching maximum anomaly values about 0.35 saltier and 1.5°C warmer than values of surrounding profiles on this isopycnal. In waters both lighter and denser than σ_θ = 26.5 kg m^{-3}, the anomaly decays, and is confined to about 26.2 < σ_θ < 26.9 kg m^{-3}.

The strongest expression of this anomalously salty (and warm) feature is located at a pressure of about 300 dbar (Fig. 2, colored contouring). Salinity values for profile 67 exceeding 35.5, obviously anomalous by visual inspection of the contoured isohalines, are limited to a 100-dbar thick region of the water column (360 < P 260 dbar). However, the entire salinity anomaly, within the density range mentioned above, has about a 160-dbar thickness (410 < P < 250 dbar). In addition, profile 67 σ_θ values are less than surrounding values for P < 300 dbar, and greater than surrounding values for P > 300 dbar (Fig. 2, white contours). In other words, the stratification around 300-dbar (in fact for about 370 > P > 240 dbar) is noticeably stronger for profile 67 than at surrounding profiles, and slightly weaker than surrounding profiles immediately above 240 dbar and below 370 dbar. This density structure clearly has dynamical implications, suggesting a cyclonic circulation with an anomalously high Π value near the core of the warm salty θ–S anomaly (P = 300 dbar and σ_θ = 26.5 kg m^{-3}).

One way to quantify the dynamic signature of the feature in profile 67 is to compute its geostrophic velocity relative to surrounding profiles. Determining a distance to use between profiles for this calculation is somewhat problematic, since there are 10.6 days between profiles, and an eddy propagating at 0.02 m s^{-1}, a typical translation velocity for anticyclonic SCVs associated with the CU (Garfield et al. 1999), could move 18 km over that time interval. However, forgoing dividing by a distance between stations during a geostrophic calculation yields a transport per unit depth between stations. The dynamic SCV signature in the density field appears to extend to about 800 dbar (not shown). Assuming zero velocity of 800 dbar results in a peak geostrophic transport per unit depth of 3270 m^2 s^{-1} at 300 dbar for profile 67 relative to surrounding profiles (Fig. 3), with values decaying toward zero in a nearly Gaussian manner above and below that pressure. The feature does not appear to have a surface expression. If a horizontal separation of 33.2 km (the distance between profiles 66 and 67) is assumed for the geostrophic calculation, a peak velocity of 0.10 m s^{-1} results at 300 dbar, whereas if a separation of 16.4 km (the distance between profiles 67 and 68) is used, the peak velocity is closer to 0.20 m s^{-1}.

Of course, for an SCV, the cyclostrophic term can also play a significant role in the dynamical balance, suggesting examination of the gradient flow that accounts for curvature in the velocity field. The larger the velocity and the smaller the radius of the SCV, the more important that term will be. For cyclonic SCVs, including the cyclostrophic term tends to reduce the velocity relative to the geostrophic estimate. Assuming a 16.4-km cyclonic radius of curvature, the velocity estimate including the cyclostrophic term is reduced to 85% of that using geostrophy alone at the vertical center

of the SCV (Fig. 3), where the reduction is largest. However, the actual impact of the cyclostrophic term is impossible to assess, as the true radius of curvature for the velocity estimates presented here is unknown. The true reduction in geostrophic velocity could be larger or smaller than that estimated here assuming a 16.4-km cyclonic radius of curvature.

Perhaps more useful than the velocity estimates, which are subject to uncertainties of what to use for a horizontal separation, are transport estimates for the SCV. A reference pressure of 800 dbar yields a geostrophic transport of 0.76×10^6 m^3 s^{-1} (Table 1). Assuming a horizontal distance of 16.4 km and including the cyclostrophic term reduces this estimate to 0.68×10^6 m^3 s^{-1}. Repeating these calculations using reference levels from 1000 to 600 dbar at 100-dbar intervals shows that while an 800-dbar reference level produces the maximum transport estimates, they are not unduly sensitive to reference level over the 600 – 1000-dbar range (Table 1). Since it is uncertain if profile 67 sampled the center of the SCV, these transport estimates might be thought of as lower bounds on the amount of water swirling around the SCV.

Data from the 370 floats that at some point during their operation reported at least two profiles as of 10 April 2008, with at least one of those profiles within the region bounded by 180°W, 10°N, 40°N, and the west coast of the Americas were examined visually in a search for other similar eddy signatures (not shown). About a dozen other subsurface features that could be interpreted as single, and often multiple, profiles taken in anticyclonic eddies were found in the almost 33,500 profiles examined. These features can be identified by a core of anomalously warm and salty water properties generally centered near $\sigma_\theta = 26.5$ kg m^{-3} and associated with anomalously low stratification. They

will be discussed elsewhere. However, no other cyclonic SCVs were evident in the Argo profile data within this geographic region.

The value of S = 34.72 on σ_θ = 26.5 kg m^{-3} within the cyclonic SCV is clearly anomalous relative to the mean map of S on that isopycnal, which estimates a value of 34.29 in the location where the SCV is observed (Fig. 4). The closest location of S = 34.72 mapped on that isopycnal is almost 1100 km due southeast of the profile. This considerable distance suggests that the cyclonic SCV must be fairly long lived.

However, the value of Π estimated for the layer $26.2 < \sigma_\theta < 26.7$ kg m^{-3} for the float profile within the cyclonic SCV is 341×10^{-12} m^{-1} s^{-1}. The SCV has a much higher core value of Π than any in the region, and the map estimates a value of 203×10^{-12} m^{-1} s^{-1} where the SCV is observed (Fig. 4). Since the SCV is cyclonic, any relative vorticity associated with it will simply increase the value of the absolute vorticity over the planetary approximation. Since Π is a conservative quantity, like θ and S on isopycnals, the origin of the cyclonic SCV becomes a bit less certain.

4. Discussion

The value of S = 32.72 on σ_θ = 26.5 kg m^{-3} within the SCV core can be found adjacent to the west coast of the Americas at least as far north as the southern end of the Gulf of California (Castro et al. 2006). The southern end of Baja California is just about 1200 km east of the cyclonic SCV. If this SCV were somehow generated in the CU, the θ–S properties suggest the CU in that region as a likely source. The amount of water swirling around the SCV and the magnitude of its core azimuthal velocity estimate are also comparable in magnitude to the transport of and core velocities within the CU.

In addition, the general tendency of eddies to propagate westward (Chelton et al. 2007) also points to this region as a likely source for the cyclonic SCV studied here. Floats in SCVs west of Monterey drifted westward at about 0.02 m s^{-1} (Garfield et al. 1999). Larger eddies with a surface signature generally propagate westward at about that speed at the latitude of Monterey, but a westward speed of 0.04 m s^{-1} might be more typical near 24°N (Chelton et al. 2007), where the cyclonic SCV studied here was observed. Using the latter propagation speed and an origin at the south end of Baja implies that the SCV may have taken about a year to reach its observed longitude.

However, the source of the anomalously large value of Π found in the cyclonic SCV is unclear. The CU core contains low Π values (Pierce et al. 2000), so the lack of valid near-coastal grid-points in the map of Π from Argo data (Fig. 4) probably does not hide unseen high Π values somewhere in the CU. The mean velocity field off Point Sur suggests a relative vorticity associated with the CU of about 0.2×10^{-5} s^{-1} given an along-shore velocity change on the order of 0.2 m s^{-1} over a cross-shore distance of 100 km (Collins et al. 2000). This value is only a few percent of the planetary value of $f = 6 \times 10^{-5}$ s^{-1} at 24°N, thus it seems unlikely that relative vorticity makes a large contribution to absolute vorticity within the CU.

The CU does shed numerous anticyclonic subsurface eddies (Garfield et al. 1999). Baroclinic instability is one likely generation mechanism for these eddies (Simpson et al. 1984; Lynn and Simpson 1990). However it is difficult to imagine how a cyclonic SCV might be shed from the CU through such an instability process.

Indeed, cyclonic subsurface vortices seem to be rare. One generation mechanism is overflow of water with high stratification, hence high Π, into a more vertically

homogenous, hence low Π, water mass: the “PV Outflow Hypothesis” (Spall and Price 1998). A mechanism along these lines is thought to generate many nearly barotropic cyclonic vortices in the Denmark Strait Overflow (Käse et al. 2003). However, no obvious analogue to this overflow exists on the west coast of the Americas to generate the cyclonic SCV observed here, and the cyclonic SCV analyzed here appears vertically compact. Its source is a puzzle.

Acknowledgments.

Float data used here were collected and made freely available by Argo (a pilot program of the Global Ocean Observing System) and contributing national programs (http://www.argo.net/). The NOAA Climate Program Office and the NOAA Office of Oceanic and Atmospheric Research supported this analysis. Kristene McTaggart pointed out the cyclonic SCV studied here. Discussions with James McWilliams were useful. The findings and conclusions in this article are those of the author and do not necessarily represent the views of the National Oceanic and Atmospheric Administration.

References

Castro, C. G., F. P. Chavez, and C. A. Collins, 2001: Role of the California Undercurrent in the export of denitrified waters from the eastern tropical North Pacific. *Global Biogeochem. Cycles*, **15**, 819-830.

Chelton, D. B., M. G. Schlax, R. M. Samelson, and R. A. de Szoeke, 2007: Global observations of large oceanic eddies. *Geophys. Res. Lett.*, **34**, L15606, doi:10.1029/2007GL030812.

Collins, C. A., C. G. Castro, H. Asuanum, T. A. Rago, S.-K. Han, R. Durazo, and F. P. Chavez, 2002: Changes in the hydrography of Central California waters associated with the 1997–98 El Niño. *Prog. Oceanogr.*, **54**, 129–147.

Collins, C. A., N. Garfield, T. A. Rago, F. W. Rischmiller, and E. Carter, 2000: Mean structure of the inshore countercurrent and California undercurrent off Point Sur, California. *Deep-Sea Res. II*, **47**, 765–782.

Durazo, R., and T. R. Baumgartner, 2002: Evolution of oceanographic conditions off Baja California: 1997-1999. *Prog. Oceanogr.*, **54**, 7–31.

Garfield, N., C. A. Collins, R. G. Paquette, and E. Carter, 1999: Lagrangian exploration of the California Undercurrent. *J. Phys. Oceanogr.*, **29**, 560–583.

Huyer, A., J. A. Barth, P. M. Kosro, R. K. Shearman, and R. L. Smith, 1998: Upper-ocean water mass characteristics of the California Current, Summer 1993. *Deep-Sea Res. II*, **45**, 1411–1442.

Jerónimo, G., and J. Gómez-Valdés, 2007: A subsurface warm-eddy of northern Baja California in July 2004. *Geophys. Res. Lett.*, **34**, L06610, doi:10.1029/2006GL028851.

Käse, R. H., J. B. Girton, and T. B. Sanford, 2003: Structure and variability of the Denmark Strait Overflow: Model and observations. *J. Geophys. Res.*, **108**, 3181, doi:10.1029/2002JC001548.

Lukas, R., and F. Santiago-Mandujano, 2001: Extreme water mass anomaly observed in the Hawaiian Ocean Time Series. *Geophys. Res. Lett.*,, **28**, 2931–2934.

Lynn, R. J., and S. J. Bograd, 2002: Dynamic evolution of the 1997–1999 El Niño–La Niña cycle in the southern California Current System. *Prog. Oceanogr.*, **54**, 59–75.

Lynn, R. J., and J. J. Simpson, 1987: The California Current system: The seasonal variability of its physical characteristics. *J. Geophys. Res.*, **92**, 12,947–12,966.

Lynn, R. J. and J. J. Simpson, 1990: The flow of the undercurrent over the continental borderland of Southern California. *J. Geophys. Res.*, **95**, 12,995–13,008.

McWilliams, J. C., 1985: Submesoscale, Coherent vortices in the Ocean. *Rev. Geophys.*, **23**, 165–182.

Pierce, S. D., R. L. Smith, P. M. Kosro, J. A. Barth, and C. D. Wilson, 2000: Continuity of the poleward undercurrent along the eastern boundary of the mid-latitude north Pacific. *Deep-Sea Res. II*, **47**, 811–829.

Simpson, J. J., T. D. Dickey, and C. J. Koblinsky, 1984: An offshore eddy in the California Current system, I, Interior dynamics. *Prog. Oceanogr.*, **13**, 5-49.

Spall, M. A., and J. F. Price, 1998: Mesoscale variability in Denmark Strait: The PV outflow hypothesis. *J. Phys. Oceanogr.*, **28**, 1598–1623.

Tables

TABLE 1. Transport estimates for the cyclonic SCV sampled by profile 67 of the Argo float with WMO #4900452. Velocities are assumed to vanish at various reference pressures. Geopotential anomaly profiles from profile 67 are differenced with the mean geopotential anomaly for profiles 65, 66, 68, and 69, then divided by the mean Coriolis parameter, *f*, for all 5 stations. The cyclostrophic estimates assume a cyclonic 16.4-km radius of curvature (the distance between profiles from cycles 67 and 68). Transports are estimated only for pressures less than the reference pressure and portions of the velocity profiles that are positive (cyclonic).

	SCV Transport Estimates $[10^6\ m^3\ s^{-1}]$	
Ref. press. [dbar]	Geostrophic	Cyclostrophic
600	0.61	0.55
700	0.67	0.63
800	0.76	0.68
900	0.70	0.60
1000	0.57	0.55

Figures

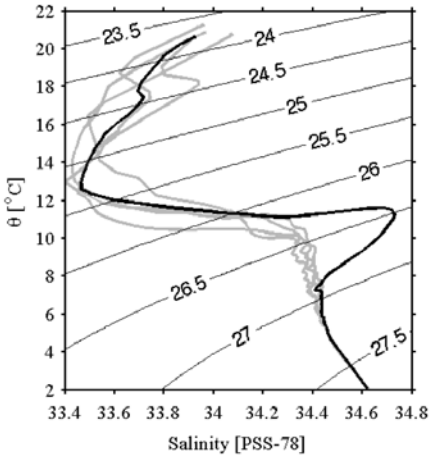

FIG. 1. Potential temperature–salinity (θ–S) curves for profiles 64-69 of the Argo float with WMO #4900452. Profile 67 (10 December 2005) is in black, and the surrounding curves from profiles 65, 66, 68, and 69 are in grey. The float has a 10.6-day cycle period. Potential density anomaly (σ_θ) is also contoured (thin labeled black lines) at 0.5 kg m^{-3} intervals.

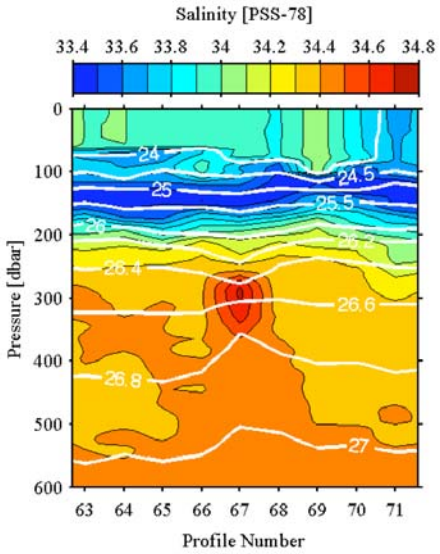

FIG. 2. Pressure–profile number section of salinity (S) for profiles 63–71 (28 October – 31 December 2005) of the Argo float with WMO #4900452, color contoured at 0.1 PSS-78 intervals (see color bar for values). Potential density anomaly (σ_θ) is also contoured (white lines with white value labels) at 0.5 kg m^{-3} intervals for $\sigma_\theta < 26$ kg m^{-3} and 0.2 kg m^{-3} intervals for $\sigma_\theta \geq 26$ kg m^{-3}.

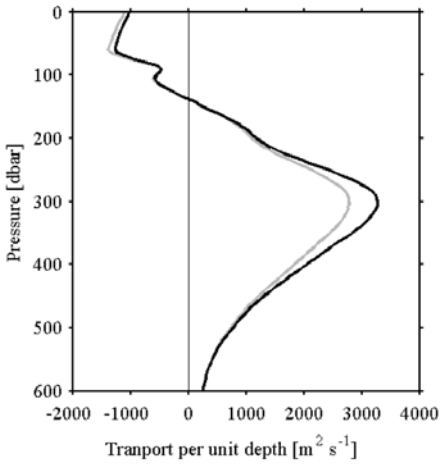

FIG. 3. Profiles of transport per unit depth [m^2 s^{-1}, cyclonic is positive] plotted versus pressure for the submesoscale coherent vortex sampled during profile 67 of the Argo float with WMO #4900452. The geostrophic estimate (black line) references geopotential anomaly profiles from the float to 800 dbar and divides the difference of the mean geopotential anomaly for profiles 65, 66, 68, and 69 and that for profile 67 by the mean Coriolis parameter, *f*, for all 5 stations. The cyclostrophic estimate (grey line) assumes a cyclonic 16.4-km radius of curvature (the distance between profiles from cycles 67 and 68).

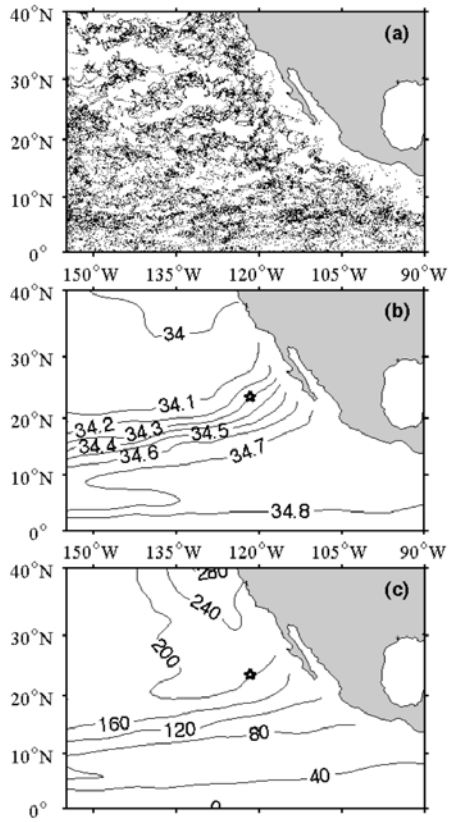

FIG. 4. (a) Location of Argo float profiles used in (b) and (c). (b) Map of salinity (S) on σ_θ = 26.5 kg m^{-3} contoured at 0.1 PSS-78 intervals. (c) Map of planetary potential vorticity (Π) estimated for the layer bounded by 26.2 < σ_θ < 26.7 kg m^{-3} calculated as detailed in Section 2 and contoured at 40 × 10^{-12} m^{-1} s^{-1} intervals. Location of the cycle 67 of WMO float 4900452 (black pentagram) is indicated on (b) and (c).